The Astrophysical Journal Letters, 992:L11 (7pp), 2025 October 10 https://doi.org/10.3847/2041-8213/ae0b56

The Impact of Alfvénic Shear Flow on Magnetic Reconnection and Turbulence

Tamar Ervin[1,2], Alfred Mallet[2], Stefan Eriksson[3], M. Swisdak[4], James Juno[5], Orlando M. Romeo[2], Tai Phan[2], Trevor A. Bowen[2], Roberto Livi[2], Phyllis L. Whittlesey[2], Davin E. Larson[2], and Stuart D. Bale[1,2]
[1] Department of Physics, University of California, Berkeley, CA 94720-7300, USA; tamarervin@berkeley.edu
[2] Space Sciences Laboratory, University of California, Berkeley, CA 94720-7450, USA
[3] Laboratory for Atmospheric and Space Physics, University of Colorado, Boulder, CO 80303, USA
[4] Institute for Research in Electronics and Applied Physics, University of Maryland, College Park, MD 20742, USA
[5] Princeton Plasma Physics Laboratory, Princeton, NJ 08543, USA
Received 2025 August 14; revised 2025 September 15; accepted 2025 September 24; published 2025 October 7

Abstract

Magnetic reconnection is a fundamental and omnipresent energy conversion process in plasma physics. Novel observations of fields and particles from Parker Solar Probe (PSP) have shown the absence of reconnection in a large number of current sheets in the near-Sun solar wind. Using near-Sun observations from PSP encounters 4–11 (2020 January–2022 March), we investigate whether reconnection onset might be suppressed by velocity shear. We compare estimates of the tearing mode growth rate in the presence of shear flow for time periods identified as containing reconnecting current sheets versus nonreconnecting times, finding systematically larger growth rates for reconnection periods. Upon examination of the parameters associated with reconnection onset, we find that 85% of the reconnection events are embedded in slow, non-Alfvénic wind streams. We compare with fast, slow non-Alfvénic, and slow Alfvénic streams, finding that the growth rate is suppressed in highly Alfvénic fast and slow wind, and reconnection is not seen in these wind types, as would be expected from our theoretical expressions. These wind streams have strong Alfvénic flow shear, consistent with the idea of reconnection suppression by such flows. This could help explain the frequent absence of reconnection events in the highly Alfvénic, near-Sun solar wind observed by PSP. Finally, we find a steepening of both the trace and magnitude magnetic field spectra within reconnection periods in comparison to ambient wind. We tie this to the dynamics of relatively balanced turbulence within these reconnection periods and the potential generation of compressible fluctuations.

Unified Astronomy Thesaurus concepts: Solar magnetic reconnection (1504); Solar wind (1534); Slow solar wind (1873)

1. Introduction

Magnetic reconnection is a ubiquitous process in plasma environments whereby magnetic energy is converted to thermal energy, heating the plasma. Evidence for magnetic reconnection is found everywhere in astrophysical (e.g., M. Hesse & P. A. Cassak 2020) and laboratory plasmas (H. Ji et al. 2023). It is a multiscale process that occurs in varied environments, from the pristine solar wind (J. T. Gosling et al. 2005) and large stellar eruptions such as coronal mass ejections and flares (J. A. Klimchuk 2006), to driving geophysical flows and the aurorae in planetary atmospheres (F. Hoyle 1949; J. Dungey 1953; J. W. Dungey 1961; X. Jia et al. 2012; G. Paschmann et al. 2013), to disrupting plasma confinement in tokamaks (H. P. Furth et al. 1963).

In addition to the importance of magnetic reconnection in driving eruptive phenomena, it is linked to other nonlinear energy conversion processes, specifically turbulence. Turbulence is known to naturally form extended current sheets (CSs; S. Boldyrev 2005; C. H. K. Chen et al. 2012; B. D. G. Chandran et al. 2015; A. Mallet et al. 2016; A. Mallet & A. A. Schekochihin 2017), which can reconnect at sufficiently small scales (N. F. Loureiro & S. Boldyrev 2017a, 2017b; A. Mallet et al. 2017a; A. Mallet et al. 2017b; D. Vech et al. 2018; C. Dong et al. 2022). A plethora of work based on simulations and observations has explored the intricacies that link these two fundamental processes, and how one process can lead to the generation of another (e.g., J. E. Stawarz et al. 2024). In situ observations provide a pathway through which we can study this.

Since its launch in 2018, Parker Solar Probe (PSP; N. J. Fox et al. 2016) has observed evidence for magnetic reconnection throughout the inner heliosphere, in CSs (T. D. Phan et al. 2020) as well as at the edges of switchback structures (C. Froment et al. 2021). However, T. D. Phan et al. (2020) also noted a lack of reconnection signatures in highly Alfvénic structures, showing that these nonreconnecting CSs had strong velocity shears. They suggested that large velocity shears might suppress reconnection, although the observed velocity shears were generally sub-Alfvénic, whereby the difference in the tangential flow velocity is less than the difference in the Alfvén velocity across the local CS. This regime had not been predicted to suppress reconnection.

A. Mallet et al. (2025) analyze the collisionless tearing-mode instability in the presence of shear flow, extending earlier work on the influence of shear on the resistive tearing mode by X. Chen & P. Morrison (1989). They find that as the flow becomes more Alfvénic and shear increases, the growth rate decreases, thus suppressing reconnection in highly Alfvénic streams. This theory could potentially explain the lack of magnetic reconnection observed in highly Alfvénic near-Sun solar wind (T. D. Phan et al. 2020; S. Eriksson et al. 2024). We

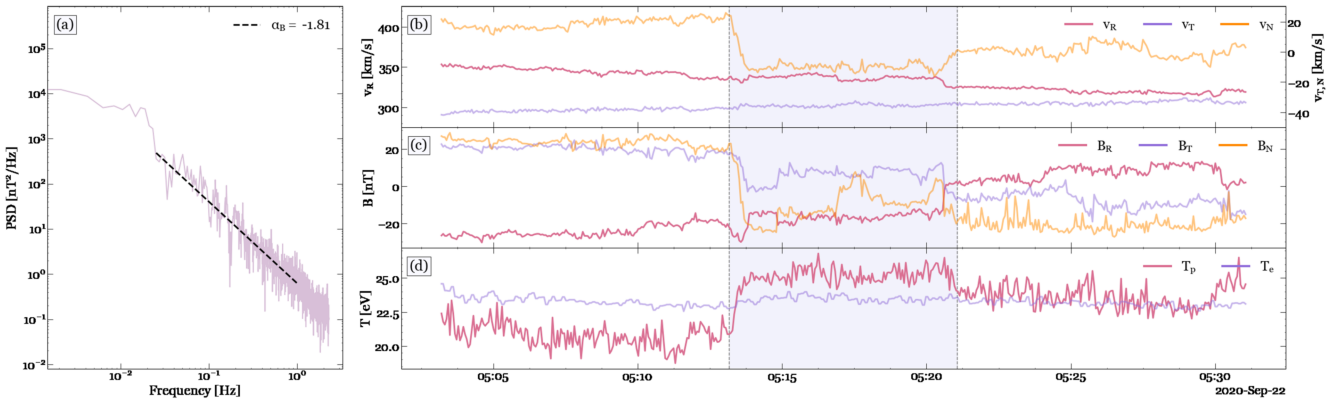

Figure 1. Overview of the fields and plasma parameters used in this study for the time period surrounding a reconnection event identified by S. Eriksson et al. (2024; highlighted in purple). Panel (a) shows the trace magnetic field spectrum and associated fit for the time period associated with the reconnection event (highlighted in panels (b–d)). The right-side panels show the (b) SPANi proton velocity, (c) FIELDS fluxgate magnetometer magnetic field measurements, and (d) ion and electron temperatures measured by the SPANi and SPANe instruments. $v_{R,T,N}$ and $B_{R,T,N}$ are the radial, tangential, and normal components of the proton velocity (b) and magnetic field (c), respectively, where R is the direction from the Sun to the spacecraft, T is the cross product of the Sun's rotation vector with R, and $N = R \times T$ (M. A. Hapgood 1992). All data have been filtered to remove time periods where the bulk of the distribution moves out of the SPANi FOV.

seek to test the analytically determined growth rate for the collisionless tearing-mode instability in the presence of shear flow as derived in A. Mallet et al. (2025) using near-Sun observations from PSP.

We will show that in periods identified as reconnection periods (RPs) by S. Eriksson et al. (2024), the shear-modified growth rate (γ_{tr}) is large relative to the maximum growth rate without shear flow (γ_{0tr}) in comparison to nonreconnection periods (NRPs), even those that are not highly Alfvénic. The ratio γ_{tr}/γ_{0tr} represents the relative suppression of tearing-mode growth rate due to the Alfvénic shear flow. It is primarily dependent on shear velocity relative to the Alfvén speed (or the Alfvén ratio) and is related to the cross helicity and residual energy. For highly Alfvénic fast and slow wind streams, we find that γ_{tr}/γ_{0tr} is much smaller than unity, pointing to suppression of reconnection due to shear flow as a potential reason for the lack of reconnection observed in near-Sun wind by PSP and note that reconnecting CSs are very rarely observed within these streams. We closely examine the plasma parameters around times identified as reconnection events, finding that the majority of the reconnection events are embedded in slow, non-Alfvénic wind.

The fact that reconnection CSs are primarily found within slow, non-Alfvénic wind streams has implications for the turbulent dynamics. Work by J. J. Podesta & J. E. Borovsky (2010) and T. A. Bowen et al. (2018) showed the impact of residual energy and cross helicity on the scaling of the turbulent spectra. We investigate the scaling of the spectral indices during these periods to compare with scalings in the ambient wind.

In Section 2 we outline our data selection methods and time periods studied. Section 3 includes discussion of our results related to the impact of Alfvénic shear flow on parameters associated with reconnection. In Section 4 we discuss our analysis of the spectral scaling and its relation to residual energy. In Section 5, we outline key conclusions and implications, including ideas for future work using this data set, and identification of areas that should be further investigated.

2. Observations

In this study, we use high cadence near-Sun observations from PSP to study the relative growth rate (γ_{tr}/γ_{0tr}) and scaling of the magnetic field spectra. Ion and electron observations are from the ion (SPANi; R. Livi et al. 2022) and electron (SPANe; P. L. Whittlesey et al. 2020) Solar Probe ANalyzers on board the "Solar Wind Electrons, Alphas, and Protons" (SWEAP; J. C. Kasper et al. 2016) suite. Electron temperatures (T_e) are determined through fitting methods of the SPANe electron distributions as described in O. M. Romeo et al. (2023) and O. M. Romeo (2024). Ion temperatures (T_i) come from the SPANi calculated moments. SPANi observations are filtered to remove time periods where the bulk of the distribution function is outside the instrument's field of view (FOV) as this leads to nonphysical and inaccurate partial moments.

Magnetic field observations come from the fluxgate magnetometer on the FIELDS instrument suite (S. D. Bale et al. 2016), providing 3D vector magnetic field measurements at high cadence. We use four samples per second cadenced measurements for our calculations. We resample FIELDS observations to the SPANi cadence (3.5 s) for our growth rate calculations and remove time periods where the bulk of the distribution is outside the SPANi FOV. We use the full-cadence magnetic field measurements for computing spectra.

We are interested in differences in the growth rate and spectral scaling between RPs and nonreconnection times. S. Eriksson et al. (2024) identified RPs using a two-step process. First, they identified unique CSs with exhaust periods that span several temporal scales. These identified periods were then checked to determine if the observed flow enhancement was consistent with a pair of propagating Alfvénic disturbances (J. T. Gosling et al. 2005). This method led to 306 candidate periods, of which 236 had confirmed reconnection exhausts. Within each of the 236 identified periods, the SPANi FOV was checked, and it was determined that the proton distribution was within the FOV of the instrument for $\geqslant$85% of the time in the majority of intervals (S. Eriksson et al. 2024). An example RP identified by S. Eriksson et al. (2024) and parameters of interest are shown in Figure 1. In this figure, you can see typical signatures of

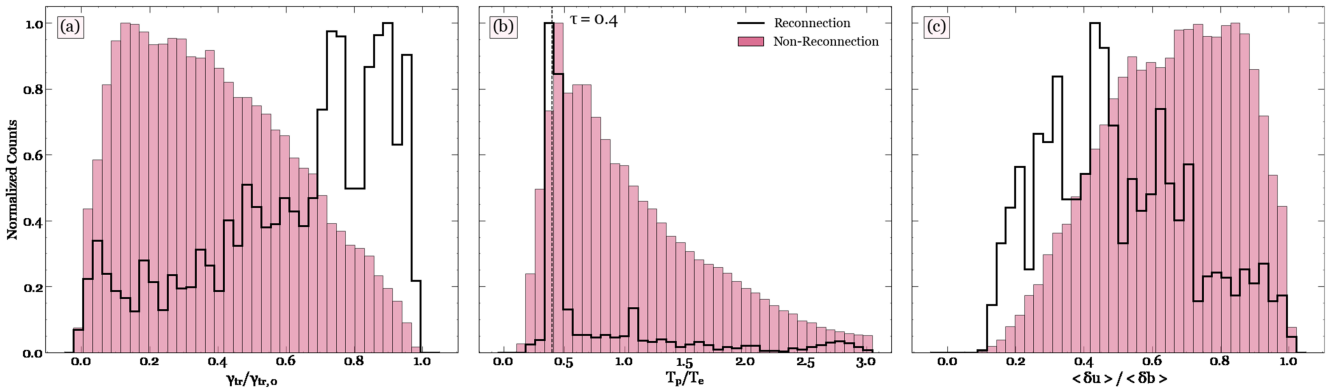

Figure 2. Comparison of (a) γ_{tr}/γ_{0tr}, (b) τ, and (c) $\sqrt{r_A} = \alpha = \langle \delta u \rangle / \langle \delta b \rangle$ for time periods associated with reconnection (black) vs. nonreconnection (pink) times. Reconnection periods are those identified by S. Eriksson et al. (2024).

reconnection such as the rotation of the field across the CS. In this specific event, we see an increase in the proton temperature while the electron temperature stays relatively constant (panel (d)).

3. Suppression of Reconnection by Alfvénic Shear Flow

To study the impact of Alfvénic shear flow on reconnection onset, we calculate the growth rate for the collisionless tearing mode in the presence of shear flow (γ_{tr}) relative to the maximum growth rate with no shear flow (γ_{0tr}). This follows the analytic expression outlined in A. Mallet et al. (2025):

$$\frac{\gamma_{tr}}{\gamma_{0tr}} = \frac{1-\alpha^2}{1+\alpha^2\tau/Z} = \frac{1-r_A}{1+r_A\tau/Z} = \frac{1-(\delta u/\delta b)^2}{1+(\delta u/\delta b)^2(T_i/T_e)/Z}, \quad (1)$$

where $\alpha = \delta u/\delta b$ is the flow shear, $\tau = T_i/T_e$, and $Z = q_i/e$. In the rest of this Letter, we discuss the Alfvén ratio (C. H. K. Chen et al. 2013) $r_A = \alpha^2 = \delta u^2/\delta b^2$ so as to not confuse the α from the growth rate expression with the spectral index (α_B) that we discuss later. In our study, we look at solely protons and electrons such that $Z = 1$ and $T_i = T_p$. δu and δb are the amplitudes of the fluctuations in the plasma velocity and Alfvén velocity. We calculate $\delta u = u - \langle u \rangle$ and $\delta b = b - \langle b \rangle$, where b is the Alfvén velocity ($b = \frac{B}{\sqrt{\mu_0 \rho}}$). ρ is calculated using a 10 minute rolling average of the proton density. $\langle \cdots \rangle$ indicates averaging of the quantity over 1 hr.

In Figure 2, we look at γ_{tr}/γ_{0tr}, τ, and $\sqrt{r_A} = \alpha$ for RPs identified by S. Eriksson et al. (2024) versus NRPs. NRPs are all background time periods within ±5 days of perihelion for encounters 4 through 11, where reconnection was not identified by S. Eriksson et al. (2024) and the proton distribution falls within our FOV requirements (O. M. Romeo et al. 2023; O. M. Romeo 2024).

We find the γ_{tr}/γ_{0tr} (panel (a)) for RPs to be much larger than for NRPs. This supports the idea that the inclusion of shear flow in the tearing-mode growth rate expression is important for correctly understanding when the growth rate is large enough such that reconnection could occur.

In panel (b), we see that $\tau = T_p/T_e$ is tightly peaked at ∼0.4 for RPs. This could point to a preferential ion-to-electron temperature ratio that is produced through magnetic reconnection. These values are calculated within the CS exhaust, rather than outside the CS, and thus point to a ratio that is a by-product of the reconnection process rather than a preferential ratio for reconnection to occur. It should be noted that we cannot directly test plasma parameters associated with reconnection onset from in situ observations. We note that some RPs show $T_p > T_e$; however, the majority show higher electron temperatures. S. Eriksson et al. (2024) note that their identified RPs are primarily embedded in wind with relatively low T_p, often seen in the slow solar wind (SSW). In comparison, the NRPs show a wide range of τ values, but the distribution is peaked near the τ peak for RPs. Additional examination of individual RPs should be conducted in a future study.

Panel (c) shows larger flow shear ($\alpha = \delta u/\delta b = \sqrt{r_A}$) values for NRPs in comparison to the RPs. This potentially indicates that flow shear can suppress reconnection in the ambient solar wind and is consistent with the theoretical idea proposed by A. Mallet et al. (2025). We expand upon this to investigate the impact of different wind types on the suppression of reconnection via flow shear.

3.1. Investigation of Relevant Plasma Parameters

Figure 3 compares the flow shear and γ_{tr}/γ_{0tr} for fast solar wind (FSW), slow Alfvénic solar wind (SASW), and classically (non-Alfvénic) SSW as identified by T. Ervin et al. (2024a). For wind categorization, the solar wind speed and cross helicity ($|\sigma_C|$; a proxy for Alfvénicity) are used. Wind is identified as "fast" or "slow" using a heliocentric-distance-based classification scheme outlined in T. Ervin et al. (2024a) and as "Alfvénic" if $|\sigma_C| \geqslant 0.7$. σ_C is calculated following the methods of T. Ervin et al. (2024a, 2024b):

$$\sigma_C = \frac{2\langle \delta \boldsymbol{u} \cdot \delta \boldsymbol{b} \rangle}{\langle \delta \boldsymbol{u}^2 \rangle + \langle \delta \boldsymbol{b}^2 \rangle} = \frac{2\sqrt{r_A}}{r_A + 1} \cos(\theta_{ub}). \quad (2)$$

Pure Alfvén waves correspond to $\sigma_C = \pm 1$, such that the turbulence is considered imbalanced. We note that σ_C is dependent upon r_A and thus is related to γ_{tr}/γ_{0tr}. We expect that highly Alfvénic wind should have a suppressed relative growth rate.

We find that γ_{tr}/γ_{0tr} for these ambient wind streams is much lower than for the RPs (Figure 2(a)). In Figure 3, we show that FSW and SASW (panels (a) and (b)) have large flow shear and, in consequence per Equation (1), small γ_{tr}/γ_{0tr}. According to the linear theory, this may explain the lack of reconnection observed by PSP in near-Sun Alfvénic wind

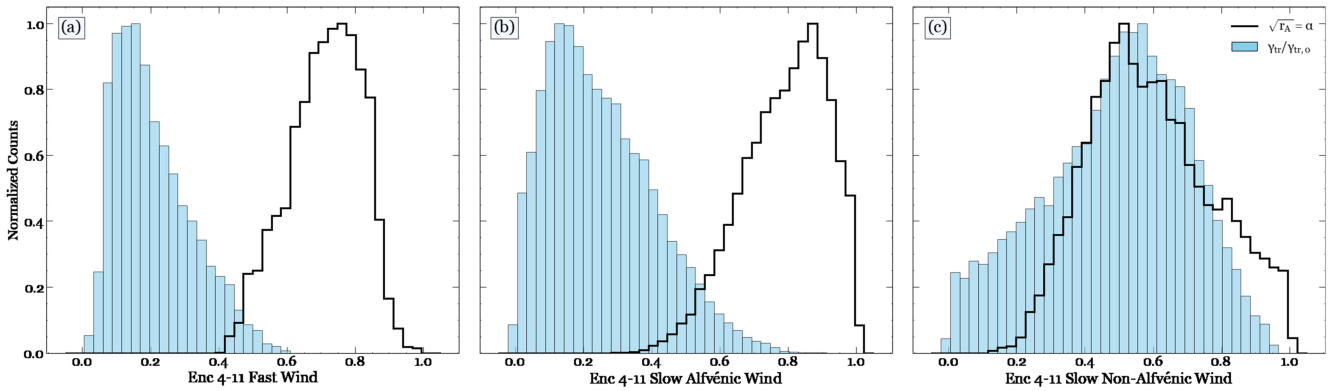

Figure 3. Comparison of γ_{tr}/γ_{0tr} (blue) and normalized flow shear (black) for (a) fast wind streams, (b) slow Alfvénic wind streams, and (c) slow wind streams. Wind is identified as fast, slow Alfvénic, or slow non-Alfvénic based on the categorization scheme of T. Ervin et al. (2024a).

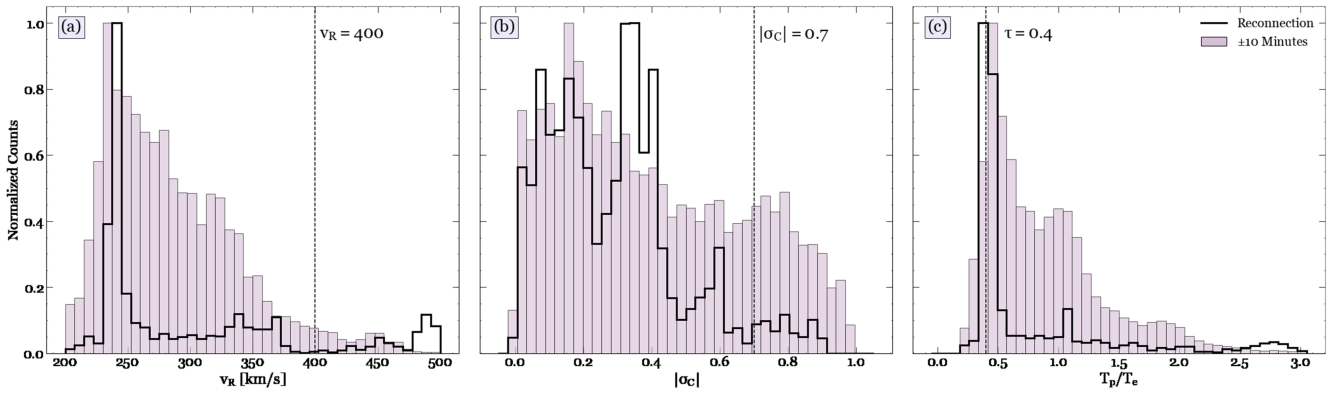

Figure 4. Comparison of (a) v_R, (b) σ_C, and (c) τ for time periods associated with reconnection (black) and ±10 minute near-reconnecting current sheet wind surrounding these events (purple).

streams. In comparison, the non-Alfvénic SSW (panel (c)) shows higher growth rates and lower shear than in the FSW and SASW. This points to RPs being more likely to be found in low-Alfvénicity, classically SSW streams. We note that the fast wind shows much larger temperature ratios ($\tau \geqslant 2$) than the slow winds ($\tau \leqslant 1.5$), regardless of Alfvénicity. This indicates that the flow shear, which as we have shown (Equations (2) and (3)) is related to the cross helicity of the plasma, is the primary parameter relevant to the growth rate.

In Figure 4, we look at the ±10 minutes time surrounding the RPs identified by S. Eriksson et al. (2024) to test this idea. We compare the velocity, cross helicity (σ_C), and temperature ratio (τ) for wind observed ±10 minutes surrounding the reconnecting periods. We refer to this ±10 minute time range as "near-reconnecting CS" (NRCS) periods. We note that the NRCS wind excludes the RPs identified by S. Eriksson et al. (2024).

In panel (a), we find that ∼96% of the NRCS wind is slow (speeds less than 400 km s^{-1}). We see a strong peak at ∼245 km s^{-1} within the reconnecting periods that could warrant further investigation. Panel (b) shows that 88% of the NRCS wind has low Alfvénicity ($|\sigma_C| \leqslant 0.7$). In combination, we find that the majority (85%) of the 236 reconnecting events that were studied are embedded within non-Alfvénic SSW streams, such that $\langle |\sigma_C| \rangle \leqslant 0.7$ and $\langle v_R \rangle \leqslant 400$ km s^{-1} where $\langle \cdots \rangle$ is the average quantity over the NRCS interval.

We show the ion-to-electron temperature ratio, τ, in panel (c), noting that the black reconnection histogram is equivalent to that shown in Figure 2. As in Figure 2, we note that there is a sharp peak at ∼0.4 within RPs, while in the NRCS periods, we see a strong peak at ∼0.45 with a larger spread. This peak is similar to the peak seen in panel (b) of Figure 2 for the ambient wind. This further supports our idea that the $\tau = T_i/T_e = 0.4$ ratio is a by-product of reconnection, rather than a preferential ratio for reconnection onset (again noting that we cannot directly test onset conditions at the X-lines with this in situ data set). The preference for RPs to be embedded in lower proton temperature wind (typical of SSW) was also noted in S. Eriksson et al. (2024).

4. Steepening of the Magnetic Field Spectral Scaling

The interplay of reconnection and turbulence is important because of the generation and disruption of small-scale CSs that can lead to dissipative heating (W. H. Matthaeus & S. L. Lamkin 1986; Y.-M. Huang & A. Bhattacharjee 2016; S. S. Cerri & F. Califano 2017; L. Franci et al. 2017; N. F. Loureiro & S. Boldyrev 2017a, 2017b; A. Mallet et al. 2017b, and others). Turbulence is often studied through the scaling of spectra calculated from in situ observations of the magnetic field, velocity field, etc. While the fast, high-cross-helicity solar wind is known to have flatter spectral scalings (C. H. K. Chen et al. 2020), the slow, low-cross-helicity solar wind has much more variation in its observed spectral indices (T. A. Bowen et al. 2018). Studies like C. Dunn et al. (2023) have shown the wide variety of fluctuation geometries that can be generated through turbulent processes. These may

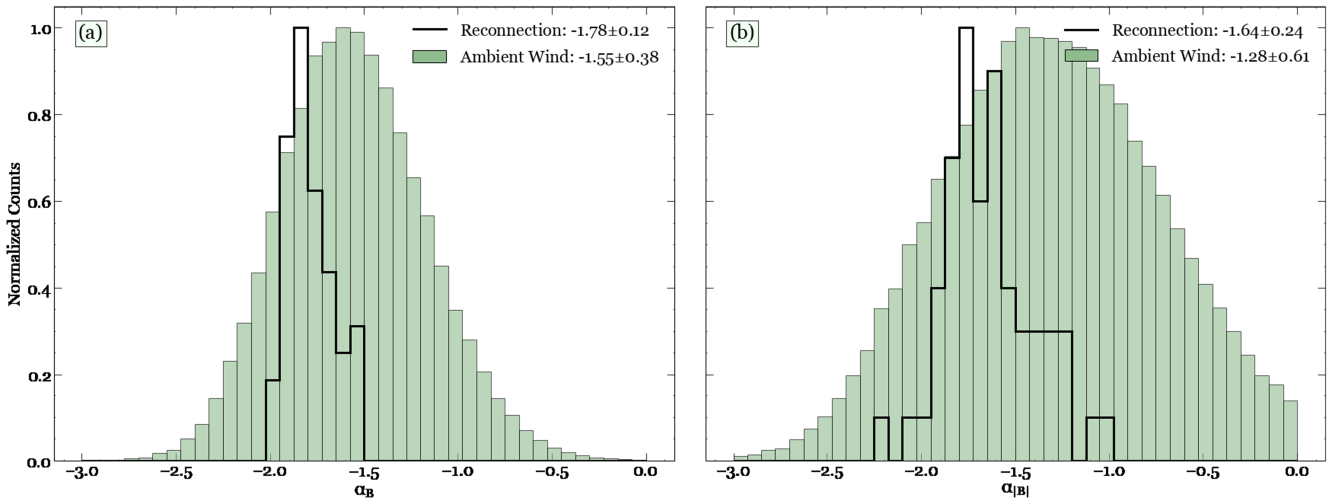

Figure 5. Comparison of magnetic field spectral index for reconnecting periods (black) identified by S. Eriksson et al. (2024) and ambient wind (green). Panel (a) shows the spectral index associated with the trace spectra (α_B) and panel (b) is the spectral index for the spectra of $|B|$ ($\alpha_{|B|}$). The legend reports the mean and standard deviation of spectral indices.

potentially be related to disruption, or other processes, perhaps associated with reconnection.

As the majority of the RPs have $\sigma_C \leqslant 0.7$, we are interested in seeing if this holds true within reconnection exhausts near the Sun and whether we can relate the generation of these steeper scalings to disruptive processes. We study the spectral index of the magnetic field spectra using PSP/FIELDS fluxgate measurements for the RPs identified by S. Eriksson et al. (2024). We look at both the trace and magnitude spectral scaling to also study the generation of compressible fluctuations.

We calculate the power spectra for reconnection time periods longer than 1 minute, using a fast Fourier transform (FFT). Trace power spectra ($\tilde{E}_B$) are calculated as a sum of the power spectra over each of the three axes, while magnitude spectra are an FFT of $|B|$ ($\tilde{E}_{|B|}$). We do a least-square fit of the spectra and frequencies in log–log space between 0.015 and 0.25 Hz where the slope of the best fit line gives the spectral index (α), whereby $E(f) \propto f^{\alpha}$. This frequency range was chosen to be far from both the outer scale and ion-scale breaks in the spectra at PSP distances, allowing us to investigate inertial range spectral scalings. We compare these indices with fits for power spectra for the ambient wind. For the ambient wind, we calculate the power spectra over 1 minute nonoverlapping windows for data ±5 days around perihelion for encounters 4 through 11 (the same time periods for NRPs discussed in Figure 2). This gives us 57 reconnection spectra for comparison with 115,348 spectra for ambient wind. In Figure 5, we show a comparison of the probability distribution for the fitted spectral indices and report the mean and standard deviation of the distributions.

We find that the trace spectral indices for the RPs are steeper ($\alpha_B \sim -1.78 \pm 0.12$) than for the ambient wind. Within reconnecting periods, the plasma has low normalized residual energy ($\sigma_R \sim -1$) and the turbulence is relatively balanced ($\sigma_C \sim 0.25$). The normalized residual energy is defined as the difference in the power of the fluctuating velocity and magnetic fields:

$$\sigma_R = \frac{\langle \delta \boldsymbol{u}^2 \rangle - \langle \delta \boldsymbol{b}^2 \rangle}{\langle \delta \boldsymbol{u}^2 \rangle + \langle \delta \boldsymbol{b}^2 \rangle} = \frac{r_{\rm A} - 1}{r_{\rm A} + 1}, \tag{3}$$

such that $\sigma_C^2 + \sigma_R^2 \leqslant 1$ geometrically. We note that, as per Equation (2), the residual energy is directly related to the γ_{tr}/γ_{0tr}, and thus periods with smaller residual energy should show lower growth rates and less reconnection.

The steeper spectral indices for RPs are consistent with results from T. A. Bowen et al. (2018), where the authors noted the dependence of the magnetic field spectral index on residual energy: as the residual energy decreased, the spectra became steeper. J. J. Podesta & J. E. Borovsky (2010) also reported a steepening of the magnetic field spectrum with decreased σ_C, though the range of values in scaling in B can vary significantly when negative residual energy is present.

In the ambient wind we find an average spectral index for the trace spectra of $\alpha_B \sim -1.55 \pm 0.38$. The majority of the ambient wind that PSP observes has $|\sigma_C| \geqslant 0.7$ and $\sigma_R \sim 0$ (T. Ervin et al. 2024a; J. Huang et al. 2025). These observations agree with the suggestions of T. A. Bowen et al. (2018), where $\alpha_B \sim -3/2$ when $\sigma_R \sim 0$.

In panel (b), we show the spectral index for the magnitude spectra ($|B|$) to look at the generation of compressible fluctuations in the solar wind. We find the spectral index within RPs $\alpha_{|B|} \sim -1.64 \pm 0.24$ to be steeper than within the ambient wind $\alpha_{|B|} \sim -1.25 \pm 0.61$. A potential reason for the steepened spectra within RPs is the generation of compressible fluctuations. C. Dunn et al. (2023) show that the presence of compressible fluctuations leads to a steepening of the $\tilde{E}_{|B|}$ spectra to $\propto f^{-5/3}$, approximately the scaling we find within the RPs. The slow wind shows large variability in plasma parameters and spectral scalings, and more work should be done to fully understand and constrain the relationship between various parameters in the slow wind and the associated spectral index.

Additional work should also be done to study the effects of reconnection on the spectral scaling of both the magnetic field and velocity spectra, and how this relates to the generation of compressible fluctuations in the solar wind. This should include the identification of additional periods to study, such that spectral scalings could be studied as a function of radial distance from the Sun (e.g., N. Sioulas et al. 2023). Investigation of the generation of steeper spectral scalings (e.g., $-8/3$ or -3) at ion scales that are theorized to be generated via reconnection processes (e.g., A. Mallet et al.

2017b) could also be done with an expanded data set and high cadence magnetic field measurements from PSP.

5. Conclusions

Through analysis of the plasma parameters and characteristics of RPs using near-Sun PSP observations, we find the following:

1. Times associated with reconnecting CSs (RPs; S. Eriksson et al. 2024) show systematically larger relative tearing-mode growth rate (γ_{tr}/γ_{0tr}) and smaller flow shear (α) than for NRPs.
2. 85% of RPs are embedded in slow non-Alfvénic wind streams with low normalized Alfvénic flow shear (equivalently, the residual energy $\sigma_r \approx -1$). This supports the theoretical ideas put forth by A. Mallet et al. (2025) that reconnection can be suppressed by Alfvénic flow shear. Highly Alfvénic slow and fast wind show large Alfvénic flow shears and small relative growth rates, with large variance in temperature ratios. This indicates that the Alfvénic flow shear is an important parameter in determining whether reconnection will occur, and could explain the suppression of reconnection observed by PSP in the near-Sun Alfvénic solar wind by shear flow.
3. Within reconnection exhausts, $\tau = T_i/T_e$ shows a small spread of values peaked at ∼0.4. This potentially indicates that reconnection may favor production of this temperature ratio, as this is the ratio within the exhaust. We note that while τ appears in the relative growth rate, its precise value may depend on the specifics of the reconnection event rather than directly reflect the upstream plasma. However, γ_{tr}/γ_{0tr} itself does not require such a specific value of τ, and so the cause of the small spread in values is left to further investigation. This should be studied in more detail looking at individual events and their associated temperature ratios.
4. We find that mean trace magnetic field spectral index within the reconnecting periods is larger than in the ambient wind. This is likely due to the impact of residual energy and the dynamics of balanced turbulence on the turbulent spectral index as discussed in T. A. Bowen et al. (2018). The magnitude spectral index within RPs is found to be steeper than in the ambient wind and consistent with scaling expected from the generation of compressive fluctuations.

Our results are consistent with the idea that with strong Alfvénic flow shear, the relative growth rate of the collisionless tearing instability is small, meaning the reconnection onset time would be increased. This could explain the absence of reconnection events in near-Sun Alfvénic wind observed by PSP, and indicates the importance of including flow shear in calculation of the tearing-mode growth rate. Further in-depth study of the plasma parameters associated with individual events is vital to obtain a full picture of magnetic reconnection in the solar wind.

It is important to note that this study did not calculate the absolute growth rate of the instability. In theory, one could calculate this absolute growth rate γ_{tr} and compare to a relevant timescale of interest, for example the nonlinear time (τ_{nl}) or the expansion time ($\tau_{\rm exp}$). It is unclear if these are the relevant timescales to understand the onset of reconnection (e.g., if $\tau_{nl}\gamma_{tr} \sim 1$ is the relevant parameter). Estimating the nonlinear timescale, for example, relies upon a detailed theory of the turbulence in the system. Given that we do not have a consensus theory for the imbalanced turbulence present in this system, and moreover that many assumptions about typical CS thicknesses and other parameters would be necessary, we have not attempted such an estimate in the present work. Future studies investigating the absolute growth rate in comparison to various timescales would be a good extension of this study to determine what is the relevant timescale and how Alfvénic shear flow impacts reconnection onset.

In balanced turbulence, where the flux of Alfvén waves parallel and antiparallel to the magnetic field is comparable ($\sigma_C \sim 0$), a range of $\delta u/\delta b$ values exist, with the peak of the $\delta u/\delta b$ distribution at significantly less than 1, similar to the reconnecting periods in this Letter (see Figure 2(c)). Thus, the suppression of reconnection by shear is not highly effective. In contrast, in imbalanced turbulence close to the Sun, where the flux of Alfvén waves is much greater in the antisunward direction than the sunward direction, $\delta u/\delta b$ is instead peaked rather close to 1, similar to the nonreconnecting periods in this Letter (see Figure 2(c)), amounting to a significant suppression of the reconnection rate. Thus, the prevalence of reconnection may depend crucially on the large-scale driving of the turbulence (e.g., whether it is balanced or imbalanced).

The fact that reconnection is suppressed in environments with strong Alfvénic shear may have broader astrophysical implications. While turbulence in the interstellar medium is likely balanced (and thus $\alpha = \delta u/\delta b \sim 0$, with little suppression of reconnection at turbulence-generated CS), other astrophysical environments, for example, accretion disk coronae and outflows (B. D. G. Chandran et al. 2018), may be heated and accelerated by imbalanced, reflection-driven turbulence, similar to the turbulent plasma observed by PSP. Based on the evidence presented here, reconnection in turbulence-generated CS may therefore be suppressed in these situations, and this may affect the character of the heating in this turbulence, with a different partitioning of energy between ions and electrons (G. G. Howes 2024). CSs in the presence of flow shear also exist at planetary magnetospheric boundaries (A. L. La Belle-Hamer et al. 1994; M. Desroche et al. 2012, 2013; G. A. Dibraccio et al. 2013; S. Eriksson et al. 2016; R. P. Sawyer et al. 2019) or downstream of quasi-parallel shocks (A. Retinò et al. 2007; T. D. Phan et al. 2018), and our results may be of use in understanding the occurrence or suppression of reconnection in these environments as well.

Acknowledgments

T.E. acknowledges funding from The Chuck Lorre Family Foundation Big Bang Theory Graduate Fellowship and NASA grant 80NSSC20K1285. A.M., S.E., and M.S. acknowledge support from NASA grant 80NSSC20K1284. J.J. was supported by the US Department of Energy under Contract No. DE-AC02-09CH1146 via LDRD grants. T.P. acknowledges support from NASA grant 80NSSC20K1781. T.A.B. acknowledges support from NASA grant 80NSSC24K0272 through the HSR program.

The FIELDS and SWEAP experiments on the Parker spacecraft were developed and are operated under NASA contract NNN06AA01C. We acknowledge the NASA Parker

Solar Probe Mission, the FIELDS team led by S. D. Bale, and the SWEAP team led by M. Stevens for use of data.

Software: `Astropy` (Astropy Collaboration et al. 2013, 2018, 2022), `matplotlib` (J. D. Hunter 2007), `numpy` (C. R. Harris et al. 2020), `pandas` (W. McKinney 2010), `pySPEDAS` (V. Angelopoulos et al. 2019), `scipy` (P. Virtanen et al. 2020), `spiceypy` (A. Annex et al. 2020).

ORCID iDs

Tamar Ervin https://orcid.org/0000-0002-8475-8606
Alfred Mallet https://orcid.org/0000-0001-9202-1340
Stefan Eriksson https://orcid.org/0000-0002-5619-1577
M. Swisdak https://orcid.org/0000-0002-5435-3544
James Juno https://orcid.org/0000-0001-6835-273X
Orlando M. Romeo https://orcid.org/0000-0002-4559-2199
Tai Phan https://orcid.org/0000-0002-6924-9408
Trevor A. Bowen https://orcid.org/0000-0002-4625-3332
Roberto Livi https://orcid.org/0000-0002-0396-0547
Phyllis L. Whittlesey https://orcid.org/0000-0002-7287-5098
Davin E. Larson https://orcid.org/0000-0001-5030-6030
Stuart D. Bale https://orcid.org/0000-0002-1989-3596

References

Angelopoulos, V., Cruce, P., Drozdov, A., et al. 2019, SSRv, 215, 9
Annex, A., Pearson, B., Seignovert, B., et al. 2020, JOSS, 5, 2050
Astropy Collaboration, Price-Whelan, A. M., Lim, P. L., et al. 2022, ApJ, 935, 167
Astropy Collaboration, Price-Whelan, A. M., Sipőcz, B. M., et al. 2018, AJ, 156, 123
Astropy Collaboration, Robitaille, T. P., Tollerud, E. J., et al. 2013, A&A, 558, A33
Bale, S. D., Goetz, K., Harvey, P. R., et al. 2016, SSRv, 204, 49
Boldyrev, S. 2005, ApJL, 626, L37
Bowen, T. A., Mallet, A., Bonnell, J. W., & Bale, S. D. 2018, ApJ, 865, 45
Cerri, S. S., & Califano, F. 2017, NJPh, 19, 025007
Chandran, B. D. G., Foucart, F., & Tchekhovskoy, A. 2018, JPlPh, 84, 905840310
Chandran, B. D. G., Schekochihin, A. A., & Mallet, A. 2015, ApJ, 807, 39
Chen, C. H. K., Bale, S. D., Bonnell, J. W., et al. 2020, ApJS, 246, 53
Chen, C. H. K., Bale, S. D., Salem, C. S., & Maruca, B. A. 2013, ApJ, 770, 125
Chen, C. H. K., Mallet, A., Schekochihin, A. A., et al. 2012, ApJ, 758, 120
Chen, X., & Morrison, P. 1989, PhFlB, 2, 495
Desroche, M., Bagenal, F., Delamere, P. A., & Erkaev, N. 2012, JGRA, 117, A07202
Desroche, M., Bagenal, F., Delamere, P. A., & Erkaev, N. 2013, JGRA, 118, 3087
Dibraccio, G. A., Slavin, J. A., Boardsen, S. A., et al. 2013, JGRA, 118, 997
Dong, C., Wang, L., Huang, Y.-M., et al. 2022, SciA, 8, eabn7627
Dungey, J. 1953, LEDPM, 44, 725
Dungey, J. W. 1961, PhRvL, 6, 47
Dunn, C., Bowen, T. A., Mallet, A., Badman, S. T., & Bale, S. D. 2023, ApJ, 958, 88
Eriksson, S., Lavraud, B., Wilder, F. D., et al. 2016, GeoRL, 43, 5606
Eriksson, S., Swisdak, M., Mallet, A., et al. 2024, ApJ, 965, 76
Ervin, T., Bale, S. D., Badman, S. T., et al. 2024b, ApJ, 972, 129
Ervin, T., Jaffarove, K., Badman, S. T., et al. 2024a, ApJ, 975, 156
Fox, N. J., Velli, M. C., Bale, S. D., et al. 2016, SSRv, 204, 7
Franci, L., Cerri, S. S., Califano, F., et al. 2017, ApJL, 850, L16
Froment, C., Krasnoselskikh, V., Dudok de Wit, T., et al. 2021, A&A, 650, A5
Furth, H. P., Killeen, J., & Rosenbluth, M. N. 1963, PhFl, 6, 459
Gosling, J. T., Skoug, R. M., McComas, D. J., & Smith, C. W. 2005, GeoRL, 32, L05105
Hapgood, M. A. 1992, P&SS, 40, 711
Harris, C. R., Millman, K. J., van der Walt, S. J., et al. 2020, Natur, 585, 357
Hesse, M., & Cassak, P. A. 2020, JGRA, 125, e25935
Howes, G. G. 2024, JPlPh, 90, 905900504
Hoyle, F. 1949, Some Recent Researches in Solar Physics (Cambridge Univ. Press: Cambridge)
Huang, J., Larson, D. E., Ervin, T., et al. 2025, ApJL, 986, L28
Huang, Y.-M., & Bhattacharjee, A. 2016, ApJ, 818, 20
Hunter, J. D. 2007, CSE, 9, 90
Ji, H., Yoo, J., Fox, W., et al. 2023, SSRv, 219, 76
Jia, X., Hansen, K. C., Gombosi, T. I., et al. 2012, JGRA, 117, A05225
Kasper, J. C., Abiad, R., Austin, G., et al. 2016, SSRv, 204, 131
Klimchuk, J. A. 2006, SoPh, 234, 41
La Belle-Hamer, A. L., Otto, A., & Lee, L. C. 1994, PhPl, 1, 706
Livi, R., Larson, D. E., Kasper, J. C., et al. 2022, ApJ, 938, 138
Loureiro, N. F., & Boldyrev, S. 2017a, ApJ, 850, 182
Loureiro, N. F., & Boldyrev, S. 2017b, PhRvL, 118, 245101
Mallet, A., Eriksson, S., Swisdak, M., & Juno, J. 2025, JPlPh, 91, E62
Mallet, A., & Schekochihin, A. A. 2017, MNRAS, 466, 3918
Mallet, A., Schekochihin, A. A., & Chandran, B. D. G. 2017a, MNRAS, 468, 4862
Mallet, A., Schekochihin, A. A., & Chandran, B. D. G. 2017b, JPlPh, 83, 905830609
Mallet, A., Schekochihin, A. A., Chandran, B. D. G., et al. 2016, MNRAS, 459, 2130
Matthaeus, W. H., & Lamkin, S. L. 1986, PhFl, 29, 2513
McKinney, W. 2010, in Proc. 9th Python in Science Conf., Data Structures for Statistical Computing in Python, 445, ed. S. van der Walt & J. Millman, 56
Paschmann, G., Øieroset, M., & Phan, T. 2013, SSRv, 178, 385
Phan, T. D., Bale, S. D., Eastwood, J. P., et al. 2020, ApJS, 246, 34
Phan, T. D., Eastwood, J. P., Shay, M. A., et al. 2018, Natur, 557, 202
Podesta, J. J., & Borovsky, J. E. 2010, PhPl, 17, 112905
Retinò, A., Sundkvist, D., Vaivads, A., et al. 2007, NatPh, 3, 236
Romeo, O. M. 2024, PhD thesis, Univ. California, Berkeley
Romeo, O. M., Braga, C. R., Badman, S. T., et al. 2023, ApJ, 954, 168
Sawyer, R. P., Fuselier, S. A., Mukherjee, J., & Petrinec, S. M. 2019, JGRA, 124, 8457
Sioulas, N., Huang, Z., Shi, C., et al. 2023, ApJL, 943, L8
Stawarz, J. E., Muñoz, P. A., Bessho, N., et al. 2024, SSRv, 220, 90
Vech, D., Mallet, A., Klein, K. G., & Kasper, J. C. 2018, ApJL, 855, L27
Virtanen, P., Gommers, R., Oliphant, T. E., et al. 2020, NatMe, 17, 261
Whittlesey, P. L., Larson, D. E., Kasper, J. C., et al. 2020, ApJS, 246, 74